

Exploring Higgs Triplet Models via Vector Boson Scattering at the LHC

Stephen Godfrey^{1,2*} and Ken Moats^{1†}

¹*Ottawa-Carleton Institute for Physics, Department of Physics, Carleton University, Ottawa, Canada K1S 5B6*

²*TRIUMF, 4004 Wesbrook Mall, Vancouver BC Canada V6T2A3*

(Dated: October 29, 2018)

We present the results of a study of Higgs triplet boson production arising in the Littlest Higgs, Left-Right Symmetric, and Georgi-Machacek models in the $W^\pm W^\pm$, $W^\pm Z$, $W^+ W^-$, and ZZ channels at the LHC. We focus on the “gold-plated” purely leptonic decay modes and consider the irreducible electroweak, QCD, and t -quark backgrounds, applying a combination of forward-jet-tagging, central-jet-vetoing, and stringent leptonic cuts to suppress the backgrounds. We find that, given the constraints on the triplet vacuum expectation value (vev), considerable luminosity is required to observe Higgs triplet bosons in vector boson scattering. Observing a Higgs triplet at the LHC is most promising in the Georgi-Machacek model due to a weaker constraint on the triplet vev. In this model, we find that a Higgs triplet boson with a mass of 1.0 (1.5) TeV can be observed at the LHC with an integrated luminosity as low as 41 (119) fb^{-1} in the $W^\pm W^\pm$ channel and as low as 171 (474) fb^{-1} in the $W^\pm Z$ channel. Observation of Higgs triplet bosons in these channels would help identify the underlying theory.

PACS numbers: 12.60.Fr, 14.80.Fd, 12.15.Ji

I. INTRODUCTION

A primary motivation for the CERN Large Hadron Collider is to understand the mechanism of electroweak symmetry breaking (EWSB) [1–3]. Related to understanding EWSB is the need for physics beyond the Standard Model (SM) to resolve the hierarchy and fine tuning problems between the electroweak scale and the Planck scale. Numerous solutions, such as Supersymmetry, Dynamical Symmetry Breaking, and Extra Dimensions, have been proposed [1–3]. An interesting class of models known as “Little Higgs” models [4] has a very rich phenomenology, including new heavy gauge bosons, new heavy quarks, and an expanded scalar sector. Much of this has been studied elsewhere [5–10] with, for the most part, the exception of the scalar sector of the theory. Would-be Goldstone multiplets are a fundamental ingredient of these theories, and the existence of scalar triplets might be a useful signature for this class of models.

It has been pointed out that doubly-charged members of the Higgs triplet ($\Phi^{\pm\pm}$) might serve as a good signal for these models if they are kinematically accessible at future colliders [6]. Han *et al.* [6] studied the effects of resonant contributions from $\Phi^{++} \rightarrow W^+ W^+$ in an idealized calculation of longitudinal $W^+ W^+$ scattering, $W_L^+ W_L^+ \rightarrow W_L^+ W_L^+$, in the Littlest Higgs model. A more detailed analysis by Azuelos *et al.* [9] found that a Φ^{++} could be observed up to 2 TeV with the right range of parameters. However, the Littlest Higgs model also predicts neutral (Φ^0) and singly-charged (Φ^\pm) members of the Higgs triplet with $W^+ W^- \Phi^0$, $ZZ \Phi^0$, and $W^+ Z \Phi^-$ interactions. If heavy scalars were observed, it would be

necessary to map out their properties to construct the underlying Lagrangian. For example, the $W^+ Z \Phi^-$ vertex is unique to Higgs triplet representations and does not exist in Two Higgs Doublet Models (2HDM), so the observation of this interaction would provide evidence for Higgs triplets [11].

The observation of a Higgs triplet state would not, however, uniquely identify the model of origin [11]. In addition to the Littlest Higgs model, scalar triplets are also included in the Georgi-Machacek model [12] and Left-Right Symmetric models [13, 14]. The so-called 3-3-1 models [15, 16] are another class of models that include Higgs triplets [17]. However, because 3-3-1 models are similar to variations of Little Higgs models, we will not consider them separately. To distinguish between models, one therefore needs to study the properties of newly discovered scalar resonances. In this paper, we study vector boson scattering to determine whether it can be used to distinguish between models that include Higgs triplet bosons. Vector boson pair production was also considered as a signature of Higgsless Models [18–23] and other possibilities for new physics [24, 25] but we do not include these scenarios in this paper.

Higgs bosons can in principle couple to fermions and, in fact, a same sign dilepton final state would almost certainly be a cleaner signal for a doubly-charged Higgs boson than vector boson final states. Although this lepton number violating decay, $\Phi^{\pm\pm} \rightarrow l^\pm l^\pm$, does not occur in the version of the Littlest Higgs model that we consider, it can occur in certain variations of the Littlest Higgs model [26], as well as in the Georgi-Machacek [27] and Left-Right Symmetric models [28–30]. It is therefore worth commenting on the relative strengths of the dilepton and VV channels. Neutrino masses are an important constraint on the allowed parameter range, which in turn leads to different decay scenarios for the Higgs triplet states [26]. In one case, the small neutrino mass

*Email: godfrey@physics.carleton.ca

†Email: kmoats@physics.carleton.ca

can be driven by a tiny triplet vacuum expectation value (vev), but with neutrino Yukawa couplings $\mathcal{O}(1)$, while in the opposite scenario it is the Yukawa couplings that are tiny to accomodate the observed neutrino masses. It is the latter case which can lead to a triplet vev that is large enough to give rise to the signal we are studying.

In this paper, we report on a study of heavy scalar triplet production via vector boson scattering in the $W^\pm W^\pm$, $W^\pm Z$, $W^+ W^-$, and ZZ channels. The models we consider are the Littlest Higgs Model, the Georgi-Machacek Model and the Left-Right Symmetric Model. We focus on the purely leptonic decays of the vector bosons, which have the advantage of lower SM QCD backgrounds. The final states we consider are therefore $W^\pm W^\pm \rightarrow l^\pm \nu l^\pm \nu$, $W^\pm Z \rightarrow l^\pm \nu l^\pm \nu$, $W^+ W^- \rightarrow l^+ \nu l^- \bar{\nu}$ and $ZZ \rightarrow l^+ l^- l^+ l^-$. These processes have been extensively studied in the context of strongly interacting weak sector models [31–34] and previous studies of doubly-charged Higgs boson production at the LHC in the Littlest Higgs and Left-Right Symmetric models were given by Azuelos *et al.* [9, 30].

In the following section, we give a brief introduction to the models we study in this paper, focusing on properties most relevant to our analysis. This is followed in Section III by a description of calculational details. In Section IV we describe possible backgrounds and the kinematic cuts that can be used to reduce them. Our results are given in Section V followed by a brief summary of our conclusions in Section VI.

II. MODELS

In this section, we give a brief overview of the Littlest Higgs, Georgi-Machacek, and Left-Right Symmetric models. It is not intended to be an extensive review but only gives details used in our analysis. The Feynman rules needed for our calculations are summarized in Table I.

A. The Littlest Higgs Model

Little Higgs models [4, 35, 36] are a class of models that attempt to resolve the hierarchy and fine-tuning problems between the electroweak scale and the Planck scale. There are many variations of Little Higgs models (for recent reviews, see [6, 7, 35, 37]). In this paper, we consider the Littlest Higgs Model [4], which introduces new particles at a scale $f \sim 1$ TeV in addition to the particles of the Standard Model. The couplings of these particles to the SM Higgs boson are such that the quadratic divergences to M_h^2 introduced by the SM loops are cancelled by the quadratic divergences introduced by the new TeV scale particles at one-loop level. As a result, the SM Higgs boson remains light and free from one-loop quadratic sensitivity up to a cutoff scale, $\Lambda_S = 4\pi f \sim 10$ TeV.

The scalar field content of the Littlest Higgs model consists of a doublet, h , and a triplet, ϕ , under the unbroken $SU(2)_L \times U(1)_Y$ Standard Model gauge group:

$$h = \begin{pmatrix} h^+ \\ h^0 \end{pmatrix}, \quad \phi = \begin{pmatrix} \phi^{++} & \phi^+/\sqrt{2} \\ \phi^+/\sqrt{2} & \phi^0 \end{pmatrix}. \quad (1)$$

Electroweak symmetry breaking results in a vev for the neutral components of both the doublet and the triplet fields: $\langle h^0 \rangle = v/\sqrt{2}$ and $\langle i\phi^0 \rangle = v'$. The doublet and triplet states acquire masses, the latter of which is given to leading order by [6]

$$M_\Phi^2 = \frac{2M_h^2 f^2}{v^2} \frac{1}{[1 - (4v'f/v^2)^2]}. \quad (2)$$

TABLE I: Feynman Rules for the interactions of scalar and vector bosons in the Littlest Higgs [6], Georgi-Machacek [27] and Left-Right Symmetric models [29].

Littlest Higgs	
$W_\mu^+ W_\nu^- h$	$\frac{i}{2} g^2 v \left(1 - \frac{v^2}{3f^2} - \frac{1}{2}(c^2 - s^2)^2 \frac{v^2}{f^2} - \frac{1}{2}s_0^2 - 2\sqrt{2}s_0 \frac{v'}{v} \right) g_{\mu\nu}$
$Z_\mu Z_\nu h$	$\frac{i}{2} \frac{g^2}{c_W^2} v \left(1 - \frac{v^2}{3f^2} - \frac{1}{2}s_0^2 + 4\sqrt{2}s_0 \frac{v'}{v} - \frac{1}{2}((c^2 - s^2)^2 + 5(c'^2 - s'^2)^2) \frac{v^2}{f^2} \right) g_{\mu\nu}$
$W_\mu^+ W_\nu^- \Phi^0$	$-\frac{i}{2} g^2 (s_0 v - 2\sqrt{2}v') g_{\mu\nu} \simeq 0$
$Z_\mu Z_\nu \Phi^0$	$-\frac{i}{2} \frac{g^2}{c_W^2} (s_0 v - 4\sqrt{2}v') g_{\mu\nu} \simeq \sqrt{2}i \frac{g^2}{c_W^2} v' g_{\mu\nu}$
$W_\mu^+ Z_\nu \Phi^-$	$-i \frac{g}{c_W} v' g_{\mu\nu}$
$W_\mu^+ h \Phi^-$	$-i \frac{g}{2} (\sqrt{2}s_0 - s_+) (p_1 - p_2)_\mu \simeq -ig \frac{v'}{v} (p_1 - p_2)_\mu$
$W_\mu^+ W_\nu^+ \Phi^{--}$	$2ig^2 v' g_{\mu\nu}$
Georgi-Machacek	
$W_\mu^+ W_\nu^- H_1^0$	$\frac{i}{2} g^2 v \left(1 - 8 \frac{v'^2}{v^2} \right) g_{\mu\nu}$
$Z_\mu Z_\nu H_1^0$	$\frac{i}{2} \frac{g^2}{c_W^2} v \left(1 - 8 \frac{v'^2}{v^2} \right) g_{\mu\nu}$
$W_\mu^+ W_\nu^- H_5^0$	$\sqrt{\frac{2}{3}} i g^2 v' g_{\mu\nu}$
$Z_\mu Z_\nu H_5^0$	$-2\sqrt{\frac{2}{3}} i \frac{g^2}{c_W^2} v' g_{\mu\nu}$
$W_\mu^+ Z_\nu H_5^-$	$-\sqrt{2}i \frac{g^2}{c_W} v' g_{\mu\nu}$
$W_\mu^+ H_1^0 H_5^-$	0
$W_\mu^+ W_\nu^+ H_5^{--}$	$2ig^2 v' g_{\mu\nu}$
$W_\mu^+ W_\nu^- H_1^{0'}$	$\frac{4}{\sqrt{3}} i g^2 v' g_{\mu\nu}$
$Z_\mu Z_\nu H_1^{0'}$	$\frac{4}{\sqrt{3}} i \frac{g^2}{c_W^2} v' g_{\mu\nu}$
Left-Right Symmetric	
$W_\mu^+ W_\nu^- h$	$\frac{i}{2} g^2 v g_{\mu\nu}$
$Z_\mu Z_\nu h$	$\frac{i}{2} \frac{g^2}{c_W^2} v g_{\mu\nu}$
$W_\mu^+ W_\nu^- \Delta_L^0$	$\sqrt{2}ig^2 v' g_{\mu\nu}$
$Z_\mu Z_\nu \Delta_L^0$	$2\sqrt{2}i \frac{g^2}{c_W^2} v' g_{\mu\nu}$
$W_\mu^+ Z_\nu \Delta_L^-$	$-i \frac{g^2}{c_W} v' g_{\mu\nu}$
$W_\mu^+ h \Delta_L^0$	0
$W_\mu^+ W_\nu^+ \Delta_L^{--}$	$-2ig^2 v' g_{\mu\nu}$

By demanding that $M_{\Phi}^2 > 0$, we arrive at a relation between the doublet and triplet vevs [4, 6]:

$$\frac{v'}{v} < \frac{v}{4f}. \quad (3)$$

For $f = 2$ TeV and $v \approx 246$ GeV, this gives an upper bound

$$v' < 8 \text{ GeV}. \quad (4)$$

The value of v' has been further constrained by electroweak data to $1 \text{ GeV} \lesssim v' \lesssim 4 \text{ GeV}$ for $f = 2$ TeV [38].

B. The Georgi-Machacek Model

The next model we consider is the Georgi-Machacek model [12], in which the scalar fields take the form

$$\phi = \begin{pmatrix} \phi^+ \\ \phi^0 \end{pmatrix}, \quad \chi = \begin{pmatrix} \chi^0 & \xi^+ & \chi^{++} \\ \chi^- & \xi^0 & \chi^+ \\ \chi^{--} & \xi^- & \chi^{0*} \end{pmatrix}, \quad (5)$$

where ϕ is a complex doublet, ξ is a real triplet and χ is a complex triplet. Electroweak symmetry breaking occurs when the neutral components of these fields develop a non-zero vev, given by $\langle \phi^0 \rangle = a/\sqrt{2}$ and $\langle \chi^0 \rangle = \langle \xi^0 \rangle = v'$. It is convenient to introduce the notation

$$v^2 \equiv a^2 + 8v'^2, \quad (6)$$

$$c_H^2 \equiv \frac{a^2}{v^2}, \quad s_H^2 \equiv \frac{8v'^2}{v^2}, \quad (7)$$

as the W^\pm and Z bosons masses are given by

$$M_W^2 = M_Z^2 \cos^2 \theta_W = \frac{1}{4} g^2 (a^2 + 8v'^2) = \frac{1}{4} g^2 v^2. \quad (8)$$

We substituted the relations given by Eqns. 6, 7 and 8 into the Feynman rules given by Ref. [27] so that the Feynman rules in Table I use a common notation.

The physical scalars in this model can be classified according to their transformation properties under the custodial $SU(2)$ symmetry, which also guarantees that $\rho = 1$ at tree-level. One finds a five-plet ($H_5^{\pm\pm}, H_5^\pm, H_5^0$), a three-plet (H_3^\pm, H_3^0), and two singlets, H_1^0 (which is identified as the SM Higgs boson) and $H_1^{0'}$. In this paper, we are interested in the production of the H_5 triplet as these particles couple to the W^\pm and Z bosons, whereas the H_3 triplet does not.

From Equation 8, we see that $v = \sqrt{a^2 + 8v'^2} \approx 246$ GeV, but the ratio v'/a is not fixed. The strongest experimental bound on this ratio comes from the $Zb\bar{b}$ coupling measurements, which give, at 95% C.L., $\tan \theta_H \equiv s_H/c_H \lesssim 0.5, 1$ and 1.7 for $M_{H_3} = 0.1, 0.5$ and 1 TeV, respectively [39]. A value of $\tan \theta_H = 0.5$ corresponds to a triplet vev of $v' = 39$ GeV, which we use in all our calculations.

C. The Left-Right Symmetric Model

The scalar sector of the $SU(2)_L \times SU(2)_R \times U(1)_{B-L}$ Left-Right Symmetric model [13, 14] is given by [29, 40]

$$\phi = \begin{pmatrix} \phi_1^0 & \phi_1^+ \\ \phi_2^- & \phi_2^0 \end{pmatrix}, \quad (9)$$

$$\Delta_L = \begin{pmatrix} \Delta_L^+/\sqrt{2} & \Delta_L^{++} \\ \Delta_L^0 & -\Delta_L^+/\sqrt{2} \end{pmatrix}, \quad (10)$$

$$\Delta_R = \begin{pmatrix} \Delta_R^+/\sqrt{2} & \Delta_R^{++} \\ \Delta_R^0 & -\Delta_R^+/\sqrt{2} \end{pmatrix}, \quad (11)$$

where left-right symmetry requires that the Lagrangian of the theory is invariant under $\Delta_L \leftrightarrow \Delta_R$ and $\phi \leftrightarrow \phi^\dagger$. The vacuum expectation values of the doublet and triplet are given by

$$\langle \phi \rangle = \frac{1}{\sqrt{2}} \begin{pmatrix} \kappa_1 & 0 \\ 0 & \kappa_2 \end{pmatrix}, \quad (12)$$

$$\langle \Delta_{L,R} \rangle = \frac{1}{\sqrt{2}} \begin{pmatrix} 0 & 0 \\ v_{L,R} & 0 \end{pmatrix}. \quad (13)$$

The triplet vevs (v_L, v_R) break $SU(2)_L \times SU(2)_R \times U(1)_{B-L} \rightarrow SU(2)_L \times U(1)_Y$, while the doublet, ϕ , breaks $SU(2)_L \times U(1)_Y \rightarrow U(1)_{EM}$.

In this paper we are interested in the production of the left triplet, Δ_L , as it couples to the Standard Model W^\pm and Z bosons. The left triplet vev, v_L , is constrained by the ρ parameter, given by [28, 29]:

$$\rho = \frac{M_W^2}{\cos^2 \theta_W M_Z^2} \simeq \frac{1 + 2v_L^2/v^2}{1 + 4v_L^2/v^2}. \quad (14)$$

The experimental result $\rho = 1.0004_{-0.0007}^{+0.0027}$ at 2σ [41] implies that $v_L \lesssim 3$ GeV, a small value compared with $v \equiv \sqrt{\kappa_1^2 + \kappa_2^2} \approx 246$ GeV. Note that due to the factor of $1/\sqrt{2}$ in Equation 13, we define the triplet vev in this model as $v' \equiv v_L/\sqrt{2}$ to be consistent with the conventions of the other models under study. Using this notation, the upper limit on the triplet vev becomes $v' \lesssim 2$ GeV.

III. CALCULATIONS

The production mechanism for scalar triplet bosons via vector boson scattering at the LHC is illustrated in Fig. 1. The incoming quarks from the colliding protons radiate vector bosons ($V = W^\pm, Z$), which interact to produce the Higgs triplet. The Higgs triplet then decays to vector bosons, accompanied by two spectator quark jets that emerge in the forward region of the detector. The forward jets are the hallmark of the vector boson fusion process and are an important tool to reduce backgrounds. We

study the production of all members of the scalar triplet: $\Phi^{\pm\pm}$ via $W^{\pm}W^{\pm}$ scattering, Φ^{\pm} via $W^{\pm}Z$ scattering, and Φ^0 via W^+W^- and ZZ scattering.

To calculate the $pp \rightarrow \Phi + jj \rightarrow VV + jj$ cross sections and kinematic distributions, we used the MadGraph software package [42]. MadGraph generates tree-level matrix elements and then generates events using Monte Carlo phase space integration. We then analyzed the generated events, including implementing kinematic cuts. We show the resulting kinematic distributions in figures and the cross sections in tables.

We implemented the relevant scalar sector Feynman rules for the Littlest Higgs model [6], the Georgi-Machacek model [27] and the Left-Right Symmetric model [29] in MadGraph (see Table I). Note that in the Littlest Higgs model, the scalar sector mixing angles are given to leading order by $s_0 = \sqrt{2}s_+ \simeq 2\sqrt{2}v'/v$ [6]. This results in a value of zero for the $W^+W^-\Phi^0$ vertex so we did not study the W^+W^- scattering process in the Littlest Higgs model. In the $WW h$ and $ZZ h$ vertices of the Littlest Higgs model, we did not include the $\mathcal{O}(v^2/f^2)$ terms in our calculations since their contributions are negligible for our purposes, regardless of the values of the mixing angles (s, c, s', c') in the gauge sector of this model.

It is interesting to note some of the similarities and differences in the Feynman rules of each model. For example, the $W^+W^+\Phi^{--}$ vertex has the same form in all three models. This is due to the fact that the doubly-charged member of the triplet has the same EW quantum numbers in each model. However, because the H_5^{\pm} of the Georgi-Machacek model is a mixture of the χ^{\pm} and ξ^{\pm} states, which have $(T_3, Y) = (0, \pm 2)$ and $(\pm 1, 0)$ respectively, this model does not have the same $W^+Z\Phi^-$ vertex as in the Littlest Higgs and Left-Right Symmetric models.

In principle, one could also use vector boson scattering to study the production of the $H_1^{0'}$ singlet in the Georgi-Machacek model. From the Feynman rules in Table I, we see that it couples more strongly to the W and Z

bosons than the H_5 triplet does. Therefore, depending on its mass, the $H_1^{0'}$ may be more easily observable in the W^+W^- and ZZ channels. Production of the $H_1^{0'}$ is also a potential background to the H_5^0 production process, which we are interested in studying. However, because we are focusing on members of the Higgs triplet, for simplicity, we do not include $H_1^{0'}$ production in our analysis.

Hadronic decays of the vector bosons have the largest branching ratios. However, the QCD backgrounds to these final states are very large and difficult to disentangle from the signal. In contrast, the purely leptonic decays, with $W^{\pm} \rightarrow l^{\pm}\nu$ and $Z \rightarrow l^+l^-$ ($l = e, \mu$), provide a much cleaner signal than hadronic decays, at the cost of a smaller branching ratio. These purely leptonic final states are often referred to as “gold-plated” modes. A final possibility is to consider semileptonic final states, sometimes referred to as “silver-plated” modes, which are intermediate in terms of branching ratios and clean final states. As expertise for reconstructing vector bosons in hadronic modes improves, these final states could prove to be useful for studying vector boson scattering. However, in this paper we focus on the “gold-plated” leptonic final states.

MadGraph includes many diagrams with the same leptonic final state as the process in which we are interested. Therefore, having MadGraph calculate the full process including decays to final state leptons includes a very large number of non-resonant diagrams and takes considerable computing time. Instead, we used MadGraph to calculate the $pp \rightarrow \Phi + jj \rightarrow VV + jj$ processes and subsequently decayed the vector bosons using the DECAY package of MadGraph. We compared cross sections and distributions using both approaches and they agreed within the statistical uncertainties of the Monte Carlo.

As a final check of our results, we calculated cross sections using the Effective Vector Boson Approximation [43] and the Goldstone Equivalence Theorem [44], and found that the two approaches were in reasonable agreement [45]. MadGraph includes a more complete set of Feynman diagrams that contributes to the final states we are studying and, more importantly, includes the spectator jets which are a crucial ingredient for reducing backgrounds.

IV. BACKGROUNDS

At the high energies associated with TeV scale Higgs boson production at the LHC, the cross section for vector boson scattering is dominated by scattering of longitudinally polarized gauge bosons, $V_L V_L \rightarrow \Phi \rightarrow V_L V_L$, where $V = W^{\pm}, Z$. Therefore, the signal process in which we are interested is

$$pp \rightarrow V_L V_L jj, \quad (15)$$

with both vector bosons decaying leptonically. In general, the experimental signature consists of high- p_T leptons in the central region of the detector, two high- p_T

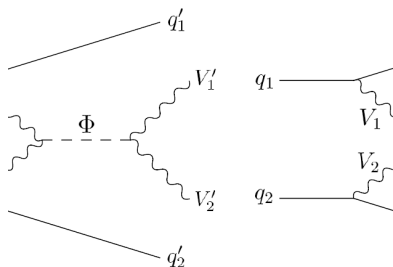


FIG. 1: Higgs triplet production via vector boson scattering at the LHC. The incoming quarks from the colliding protons radiate vector bosons, which interact to produce a Higgs triplet as an s-channel resonance. Two vector bosons emerge in the final state, along with two forward spectator quark jets.

forward jets and low jet activity in the central region. We consider three types of backgrounds to this signal following the treatment of [31–33].

The first background is the irreducible electroweak (EW) background. It is similar to the signal process except that at least one of the vector bosons is transversely polarized:

$$pp \rightarrow V_T V_L jj, \quad (16)$$

$$pp \rightarrow V_T V_T jj. \quad (17)$$

This process is a background in the sense that its cross section is essentially insensitive to the new TeV scale physics that we wish to study. It is irreducible in the sense that the final state is virtually identical to the signal process, differing only by the polarization of the vector bosons, making this background difficult to reduce using simple kinematic cuts. In principle, if one could distinguish between the final state vector boson polarizations, this background could be considerably reduced. A recent paper by Han *et al.* argues that this can be done [46]. In any case, we find that the cuts we implement reduce this background to a manageable level. We therefore define our signal cross section for TeV scale Higgs boson production through vector boson scattering as

$$\begin{aligned} \sigma_{\text{signal}}(pp \rightarrow V_L V_L jj) \\ \equiv \sigma_{\text{total}}(pp \rightarrow VVjj) - \sigma_{SM}(pp \rightarrow VVjj), \end{aligned} \quad (18)$$

where $\sigma_{SM}(pp \rightarrow VVjj)$ is the cross section for the EW background process of the Standard Model, and $\sigma_{\text{total}}(pp \rightarrow VVjj)$ includes the contributions from the Higgs triplet model under consideration.

The second class of background processes are QCD backgrounds, which involve the production of two vector bosons plus additional jets:

$$pp \rightarrow VV + nj, \quad (19)$$

where n is the number of jets in the final state, typically with $n = 2$. We also include the 1-jet background because we only tag one forward jet in our analysis. It is possible to tag two high- p_T forward jets, but such double tagging has been shown to be too costly to the number of signal events [31]. Therefore, we choose to tag a single forward jet in our analysis, as this retains a larger fraction of the signal events.

We evaluate these backgrounds to order $\mathcal{O}(\alpha^2 \alpha_s^n)$, where $n = 1$ or 2 , in contrast to the irreducible EW background, which is of order $\mathcal{O}(\alpha^4)$. Since the VV scattering signal is a purely electroweak process with no colour exchange and relatively low jet activity in the central region, the jets arising in the QCD background are generally more central and have higher p_T than the spectator jets from the signal events. Therefore, in addition to a forward jet tag, imposing a central jet veto to reject events with hard central jets is very useful in reducing the QCD background.

The third type of background we consider includes top quarks in the final state, generally along with a vector

boson and possibly an additional jet:

$$pp \rightarrow V t \bar{t}, \quad (20)$$

$$pp \rightarrow V t \bar{t} j. \quad (21)$$

These backgrounds arise from the leptonic decays of the vector boson, $V = W^\pm$ or Z , along with the t and \bar{t} decaying into real W bosons, which then decay leptonically or hadronically. The resulting final state can have many leptons and jets that can mimic the signal. Fortunately, unlike the jets from the signal process, the jets from the t -quark background tend to emerge in the central region of the detector. Therefore, the t -quark background can also be suppressed by imposing a forward jet tag and a central jet veto.

In the following subsections we give a more detailed description of the backgrounds to each of the final states and the kinematic cuts we use to reduce them to manageable levels.

A. $W^\pm W^\pm$

The SM backgrounds to the $W^\pm W^\pm$ channel are:

- EW Background:

$$pp \rightarrow W^\pm W^\pm jj, \mathcal{O}(\alpha^4) \quad (22)$$

- QCD Background:

$$pp \rightarrow W^\pm W^\pm jj, \mathcal{O}(\alpha^2 \alpha_s^2) \quad (23)$$

- Top Quark Background:

$$pp \rightarrow W^\pm t \bar{t}, \quad (24)$$

$$pp \rightarrow W^\pm t \bar{t} j, \quad (25)$$

with $t \rightarrow Wb$.

- $W^\pm Z$ Background:

$$pp \rightarrow W^\pm Z + nj \quad (26)$$

with the W^\pm and Z decaying leptonically, $W^\pm Z \rightarrow l^\pm \nu l^+ l^-$. This process is a background to the $W^\pm W^\pm$ signal if the l^\mp from the Z decay is not observed, due to the finite coverage of the EM calorimeter. We therefore include all the EW, QCD and t -quark backgrounds to the $W^\pm Z$ channel as backgrounds to the $W^\pm W^\pm$ channel.

We include the $W^+ W^+$ final state as well as the charge-conjugate $W^- W^-$ final state to enhance our statistics in this channel. Note that the cross sections for the two charge-conjugate channels are not identical due to different parton distribution functions contributing to the different charge states.

For the $W^\pm W^\pm$ channel, the leptonic decay mode in which we are interested is $W^\pm W^\pm \rightarrow l^\pm \nu l^\pm \nu$, where

$l = e, \mu$. Because of the neutrinos in the final state, the W boson pair cannot be fully reconstructed. Therefore, we consider the cluster transverse mass of the WW pair [33, 47, 48] rather than the WW invariant mass distribution. In general, for a pair of vector bosons decaying leptonically, we define the cluster transverse mass as

$$M_T^2(VV) = \left[E_T^{\text{leptons}} + \cancel{E}_T \right]^2 - \left[\mathbf{p}_T^{\text{leptons}} + \mathbf{\cancel{p}}_T \right]^2 \quad (27)$$

where $E_T = \sqrt{M^2 + p_T^2}$, and M is the invariant mass. Therefore, the WW cluster transverse mass is given by

$$M_T^2(WW) = \left[\sqrt{M^2(ll) + p_T^2(ll)} + \sqrt{M^2(\nu\nu) + |\mathbf{\cancel{p}}_T|^2} \right]^2 - [\mathbf{p}_T(ll) + \mathbf{\cancel{p}}_T]^2 \quad (28)$$

where $\mathbf{p}_T(ll) = \mathbf{p}_T(l_1) + \mathbf{p}_T(l_2)$. However, since the invariant mass of the two neutrinos, $M(\nu\nu)$, cannot be reconstructed, we instead define the WW cluster transverse mass as

$$M_T^2(WW) = \left[\sqrt{M^2(ll) + p_T^2(ll)} + |\mathbf{\cancel{p}}_T| \right]^2 - [\mathbf{p}_T(ll) + \mathbf{\cancel{p}}_T]^2. \quad (29)$$

With this definition, the production of a doubly-charged Higgs boson through $W^\pm W^\pm$ scattering results in a broad peak in the $M_T(WW)$ distribution with an endpoint at approximately the resonance mass. This can clearly be seen in Fig. 3 for the $M_\Phi = 1$ TeV case, while the broader $\Phi^{\pm\pm}$ width for the $M_\Phi = 1.5$ TeV case smears out the $M_T(WW)$ distribution.

B. $W^\pm Z$

In the $W^\pm Z$ channel, we consider the following SM backgrounds:

- EW Background:

$$pp \rightarrow W^\pm Z jj, \mathcal{O}(\alpha^4) \quad (30)$$

- QCD Background:

$$pp \rightarrow W^\pm Z j, \mathcal{O}(\alpha^2 \alpha_s) \quad (31)$$

$$pp \rightarrow W^\pm Z jj, \mathcal{O}(\alpha^2 \alpha_s^2) \quad (32)$$

- Top Quark Background:

$$pp \rightarrow Z t \bar{t}, \quad (33)$$

$$pp \rightarrow Z t \bar{t} j, \quad (34)$$

with $t \rightarrow Wb$.

Note that we consider the $W^+ Z$ final state as well as the charge-conjugate $W^- Z$ final state to enhance our statistics in this channel.

Using Equation 27, we obtain the WZ cluster transverse mass:

$$M_T^2(WZ) = \left[\sqrt{M^2(lll) + p_T^2(lll)} + |\mathbf{\cancel{p}}_T| \right]^2 - [\mathbf{p}_T(lll) + \mathbf{\cancel{p}}_T]^2. \quad (35)$$

The $M_T(WZ)$ distribution for singly-charged Higgs boson production through WZ scattering shows a distinctive peak at the resonance mass, as seen in Fig. 4.

C. $W^+ W^-$

In the $W^+ W^-$ channel, we consider the following SM backgrounds:

- EW Background:

$$pp \rightarrow W^+ W^- jj, \mathcal{O}(\alpha^4) \quad (36)$$

- QCD Background:

$$pp \rightarrow W^+ W^- j, \mathcal{O}(\alpha^2 \alpha_s) \quad (37)$$

$$pp \rightarrow W^+ W^- jj, \mathcal{O}(\alpha^2 \alpha_s^2) \quad (38)$$

- Top Quark Background:

$$pp \rightarrow t \bar{t}, \quad (39)$$

$$pp \rightarrow t \bar{t} j, \quad (40)$$

with $t \rightarrow Wb$.

The $W^\pm Z$ scattering process may also be a background to the $W^+ W^-$ channel if the l^\pm from the Z decay is not detected. However, this is far less important than the large QCD and t -quark backgrounds to $W^+ W^-$ scattering, so it will be neglected.

As in the $W^\pm W^\pm$ channel, the $W^+ W^-$ invariant mass cannot be fully reconstructed for leptonic final states, so instead we use the $W^+ W^-$ cluster transverse mass, also given by Equation 29.

D. ZZ

In the ZZ channel, we consider the following SM backgrounds:

- EW Background:

$$pp \rightarrow ZZjj, \mathcal{O}(\alpha^4) \quad (41)$$

- QCD Background:

$$pp \rightarrow ZZj, \mathcal{O}(\alpha^2\alpha_s) \quad (42)$$

$$pp \rightarrow ZZjj, \mathcal{O}(\alpha^2\alpha_s^2) \quad (43)$$

An advantage of the $ZZ \rightarrow 4l$ decay mode is that we can completely reconstruct the final state and make use of the ZZ invariant mass distribution in our results.

E. Kinematic Cuts

The kinematic cuts used to reduce the SM backgrounds to vector boson scattering are well established [31–34]. Our values for the cuts are summarized in Table II. We impose cuts on the p_T of all charged leptons, the missing transverse momentum (\cancel{p}_T) in the $W^\pm Z$ channel, and impose back-to-back lepton cuts ($\Delta y(l)$ and $\Delta p_T(l)$) in the $W^\pm W^\pm$ and W^+W^- channels. We impose rapidity cuts on the final state leptons of $|y(l)| < 2.5$ and on the tag jet of $3.0 < |y(j_{tag})| < 5.0$ to take into account detector acceptances. Imposing a central jet veto was not necessary in the ZZ channel, as this would further reduce the already small number of signal events. Note that the central jet veto cuts are to be interpreted as: “Reject all events with jets having $|y| < y_{max}$ and $p_T > p_{Tmin}$ ”. It should also be noted that, although we tag a single energetic forward jet with high- p_T , all jets are assumed to have $p_T > 10$ GeV by default. This is required in order for MadGraph to achieve stable results in its calculations. We find that these choices of cuts are effective in improving the signal to background ratio.

V. RESULTS

We used the MadGraph software package [42], version 4.2.6, to generate weighted signal and background events. To obtain our results, we used the following SM input parameters [41]: $G_F = 1.16637 \times 10^{-5}$ GeV⁻², $M_Z = 91.188$ GeV, $\alpha(M_Z) = 1/127.9$, $\alpha_s(M_Z) = 0.118$, $M_t = 171.2$ GeV. We assumed a SM Higgs boson mass of $M_h = 120$ GeV and used the CTEQ6M parton distribution functions [49]. We assumed the nominal LHC energy of $\sqrt{s} = 14$ TeV and an integrated luminosity of $\mathcal{L} = 100$ fb⁻¹ to obtain our results.

In the Higgs triplet models that we studied, there are additional parameters in the scalar sector that must be defined. For all models, we use triplet masses of

TABLE II: Leptonic cuts and jet cuts used in vector boson scattering to enhance the signal to background ratio. Note that the central jet veto cuts are to be interpreted as: “Reject all events with jets having $|y| < y_{max}$ and $p_T > p_{Tmin}$ ”.

Leptonic Cuts	Jet Cuts
$W^\pm W^\pm$	
$ y(l) < 2.5$	$3.0 < y(j_{tag}) < 5.0$
$p_T(l_1) > 200$ GeV	$p_T(j_{tag}) > 40$ GeV
$p_T(l_2) > 50$ GeV	$E(j_{tag}) > 500$ GeV
$\Delta p_T(l) = p_T(l_1) - p_T(l_2) > 300$ GeV	$ y(j_{veto}) < 3.0$
$\Delta y(l) = y(l_1) - y(l_2) < 3$	$p_T(j_{veto}) > 100$ GeV
$M_T(WW) > 550$ (800) GeV	
for $M_\Phi = 1.0$ (1.5) TeV	
$W^\pm Z$	
$ y(l) < 2.5$	$3.0 < y(j_{tag}) < 5.0$
$p_T(l_1) > 150$ GeV	$p_T(j_{tag}) > 40$ GeV
$p_T(l_2) > 50$ GeV	$E(j_{tag}) > 500$ GeV
$p_T(l_3) > 50$ GeV	$ y(j_{veto}) < 3.0$
$\cancel{p}_T > 50$ GeV	$p_T(j_{veto}) > 100$ GeV
$M_T(WZ) > 900$ (1250) GeV	
for $M_\Phi = 1.0$ (1.5) TeV	
W^+W^-	
$ y(l) < 2.5$	$3.0 < y(j_{tag}) < 5.0$
$p_T(l_1) > 300$ GeV	$p_T(j_{tag}) > 40$ GeV
$p_T(l_2) > 150$ GeV	$E(j_{tag}) > 800$ GeV
$\Delta p_T(l) = p_T(l_1) - p_T(l_2) > 500$ GeV	$ y(j_{veto}) < 3.0$
$\Delta y(l) = y(l_1) - y(l_2) < 3$	$p_T(j_{veto}) > 60$ GeV
$M_T(WW) > 700$ (1000) GeV	
for $M_\Phi = 1.0$ (1.5) TeV	
ZZ	
$ y(l) < 2.5$	$3.0 < y(j_{tag}) < 5.0$
$p_T(l) > 70$ GeV	$p_T(j_{tag}) > 40$ GeV
$M(ZZ) > 900$ (1250) GeV	$E(j_{tag}) > 500$ GeV
for $M_\Phi = 1.0$ (1.5) TeV	
no jet veto	

$M_\Phi = 1.0$ and 1.5 TeV and a triplet vev of $v' = 39$ GeV; as discussed in Section II, this value of the triplet vev corresponds to the upper bound in the Georgi-Machacek model. In the Littlest Higgs model, the symmetry breaking scale, f , is an additional parameter that we set to $f = 2$ TeV. With these parameter values, we used the BRIDGE [50] package of MadGraph to calculate the scalar triplet decay widths for each of the models, and the resulting values are given in Table III.

For the purpose of discussion we start with $W^\pm Z$ scattering as a representative case. The process is $pp \rightarrow W^\pm Zjj$ with, for the “gold-plated” leptonic decay modes, $W^\pm \rightarrow l^\pm \nu$ and $Z \rightarrow l^+ l^-$ ($l = e, \mu$). The experimental signature is given by two high- p_T forward jets, along with three high- p_T charged leptons in the central region of the detector. This is accompanied by a large

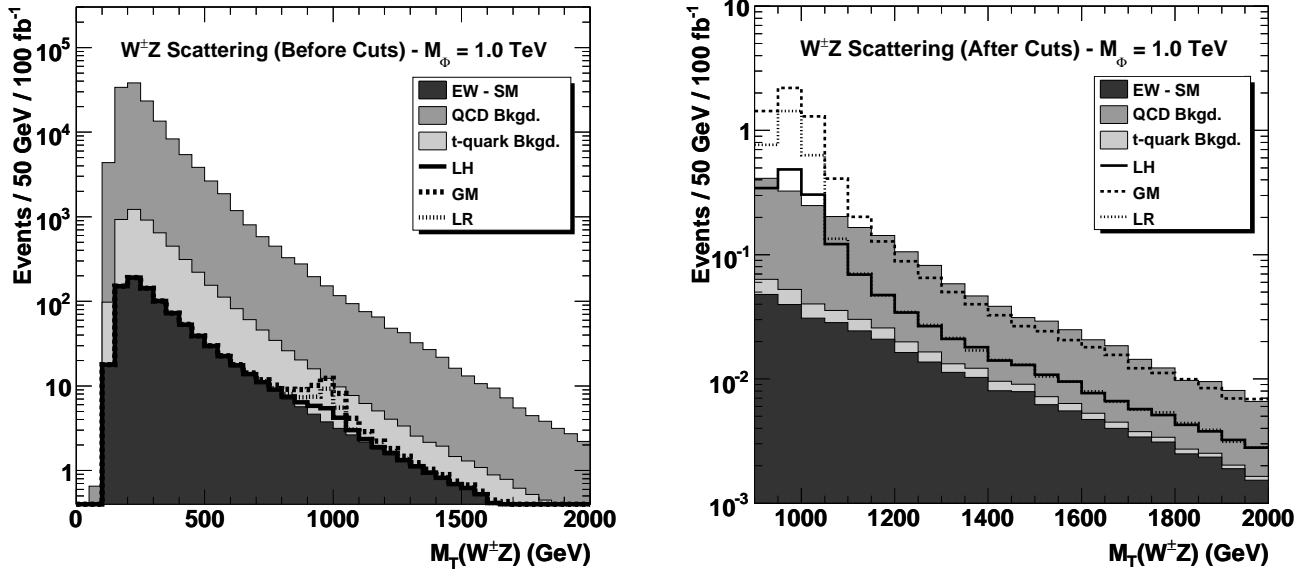


FIG. 2: The transverse mass distributions for the $W^\pm Z$ signals of the Littlest Higgs (LH), Georgi-Machacek (GM) and Left-Right Symmetric (LR) models, along with the backgrounds, before and after imposing the cuts of Table II. A Higgs triplet mass of $M_\Phi = 1.0$ TeV was used, along with a triplet vev of $v' = 39$ GeV, assuming an integrated luminosity of $\mathcal{L} = 100 \text{ fb}^{-1}$. Note that the backgrounds are stacked, whereas the signal lines are not.

amount of missing p_T attributed to the undetected neutrino. The transverse mass distributions for each type of background along with the $W^\pm Z$ signal before and after imposing the cuts of Table II are shown in Fig. 2, for a triplet mass of $M_\Phi = 1.0$ TeV. It can be seen from this figure that our choice of cuts reduces the irreducible EW background to a manageable level and substantially reduces the QCD and t -quark backgrounds.

All channels show qualitatively similar improvements in the signal to background ratio, so for the remaining channels we simply show the resulting mass distributions after imposing the kinematic cuts given in Table II. The resulting cluster transverse mass distributions for the $W^\pm W^\pm$, $W^\pm Z$, and $W^+ W^-$ channels, and the invariant mass distribution for the ZZ channel are shown in Figs. 3-6 for $M_\Phi = 1.0$ and 1.5 TeV.

To better understand these plots, it is helpful to refer to the scalar triplet partial widths in these models, which are given in Table III. We start with the $W^\pm W^\pm$ channel shown in Fig. 3. The transverse mass distributions for all three models in the $W^\pm W^\pm$ channel lie on top of each other because the doubly-charged member of the scalar triplet has identical $W^+ W^+ \Phi^{--}$ vertices and the same decay width in each model. In contrast, the $W^\pm Z$ channel, shown in Fig. 4, exhibits differences between all three models. The peak width for the Littlest Higgs model signal is larger than that of the Left-Right Symmetric model signal because, although they have the same $W^+ Z \Phi^-$ vertex, the Φ^\pm of the Littlest Higgs model

can also decay to $W^\pm h$, resulting in a larger Φ^\pm width. Furthermore, although the H_5^\pm of the Georgi-Machacek model can only decay to $W^\pm Z$, as discussed previously, the $W^+ Z H_5^-$ coupling is larger by a factor of $\sqrt{2}$ compared to the $W^+ Z \Delta_L^-$ coupling in the Left-Right Symmetric model, resulting in a H_5^\pm width that is a factor of two larger than the Δ_L^\pm width and also a larger production cross section. Finally, the differential cross sections in the ZZ channel shown in Figure 6 differ quite significantly due to the different $\Phi^0 ZZ$ couplings and Φ^0 widths. The width of the neutral member of the scalar triplet is smallest in the Littlest Higgs model, partially due to the absence of the $\Phi^0 \rightarrow W^+ W^-$ decay mode at leading order in this model, but also due to the value of the $\Phi^0 ZZ$ coupling. In both the GM and LR models the Φ^0 can also decay $W^+ W^-$ which increases the total width. These effects are not so apparent in the $W^+ W^-$ channel because the signal is more deeply buried in the background.

More quantitatively, in Table IV we give the cross sections for the signal and backgrounds after imposing the cuts of Table II. We show cross sections for the Littlest Higgs model, the Georgi-Machacek model, and the Left-Right Symmetric model for scalar triplet masses of $M_\Phi = 1.0$ and 1.5 TeV. The row labelled as EW-SM is the Standard Model cross section, assuming a Higgs mass of $M_h = 120$ GeV, which we refer to in the text as the irreducible EW background. The rows labelled as Signal-LH, Signal-GM, and Signal-LR are the difference

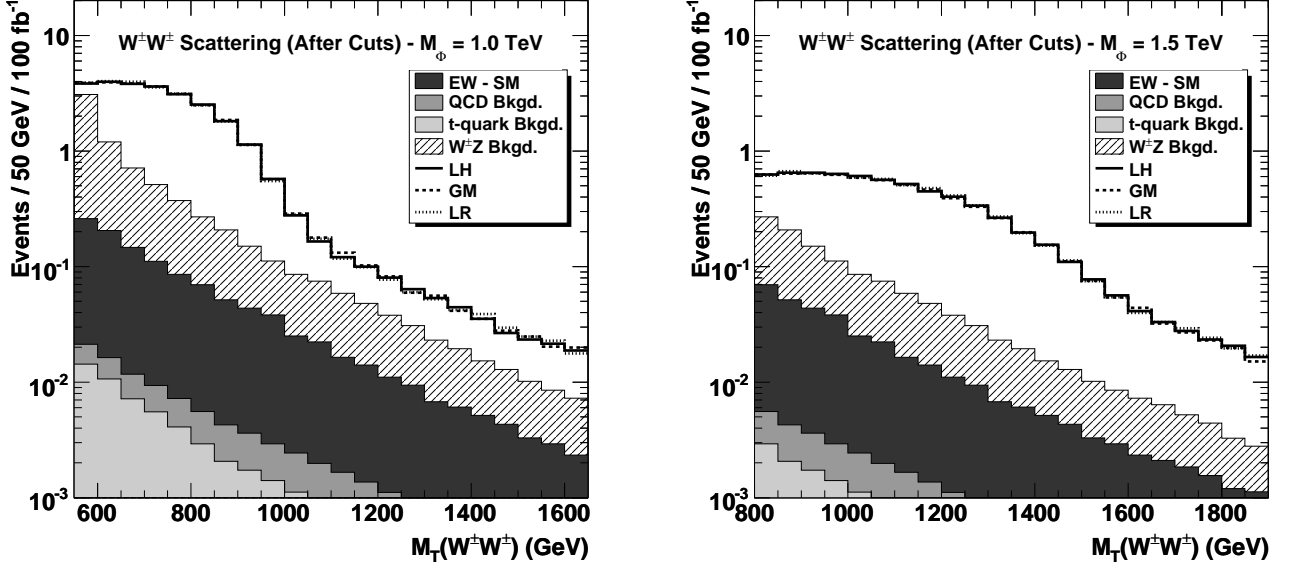


FIG. 3: The transverse mass distributions for $W^\pm W^\pm$ scattering in the Littlest Higgs (LH), Georgi-Machacek (GM) and Left-Right Symmetric (LR) models, along with the backgrounds, after imposing the cuts of Table II. Higgs triplet masses of $M_\Phi = 1.0$ and 1.5 TeV were used, along with a triplet vev of $v' = 39$ GeV, assuming an integrated luminosity of $\mathcal{L} = 100 \text{ fb}^{-1}$. Note that the backgrounds are stacked, whereas the signal lines are not.

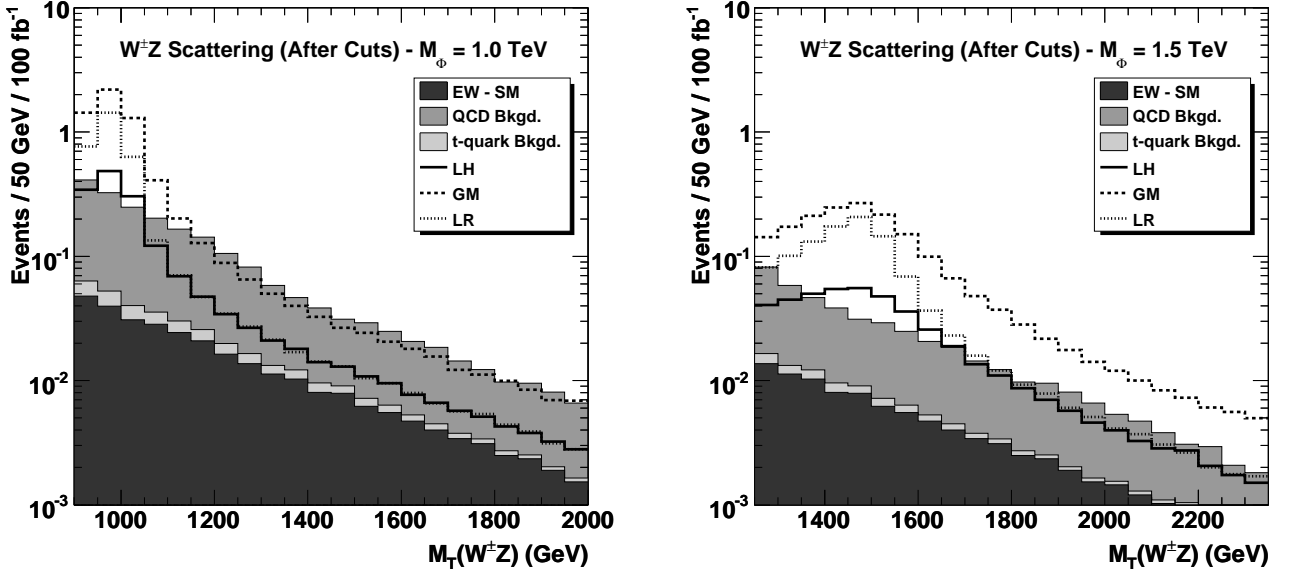


FIG. 4: The transverse mass distributions for $W^\pm Z$ scattering in the Littlest Higgs (LH), Georgi-Machacek (GM) and Left-Right Symmetric (LR) models, along with the backgrounds, after imposing the cuts of Table II. Higgs triplet masses of $M_\Phi = 1.0$ and 1.5 TeV were used, along with a triplet vev of $v' = 39$ GeV, assuming an integrated luminosity of $\mathcal{L} = 100 \text{ fb}^{-1}$. Note that the backgrounds are stacked, whereas the signal lines are not.

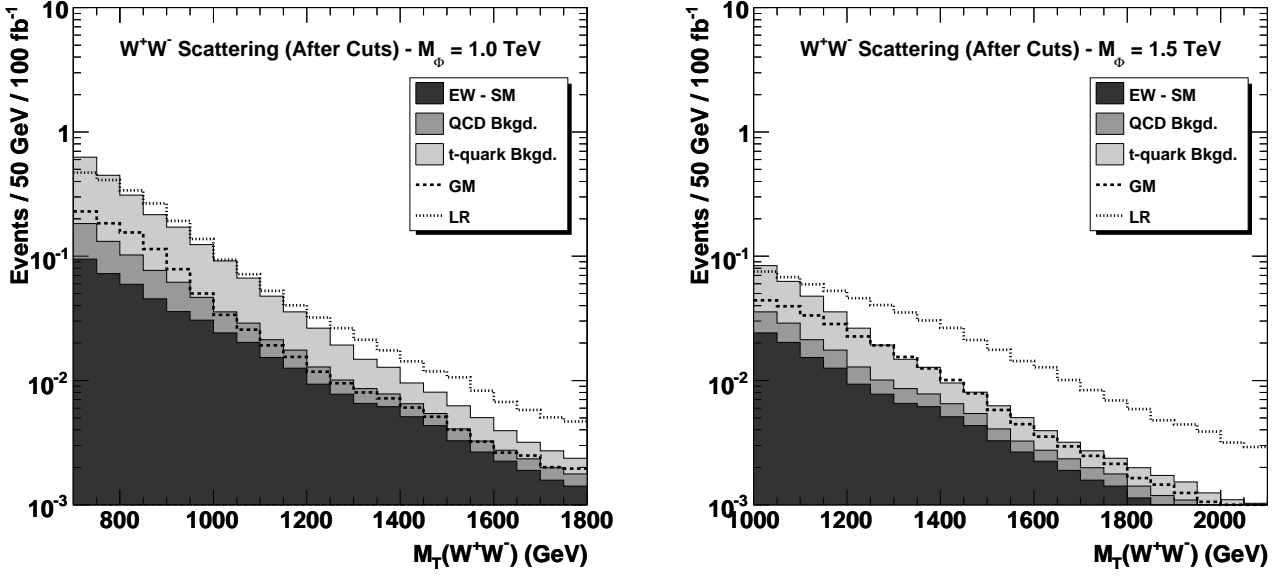


FIG. 5: The transverse mass distributions for W^+W^- scattering in the Georgi-Machacek (GM) and Left-Right Symmetric (LR) models (this signal does not exist in the Littlest Higgs model at lowest order), along with the backgrounds, after imposing the cuts of Table II. Higgs triplet masses of $M_\Phi = 1.0$ and 1.5 TeV were used, along with a triplet vev of $v' = 39$ GeV, assuming an integrated luminosity of $\mathcal{L} = 100 \text{ fb}^{-1}$. Note that the backgrounds are stacked, whereas the signal lines are not.

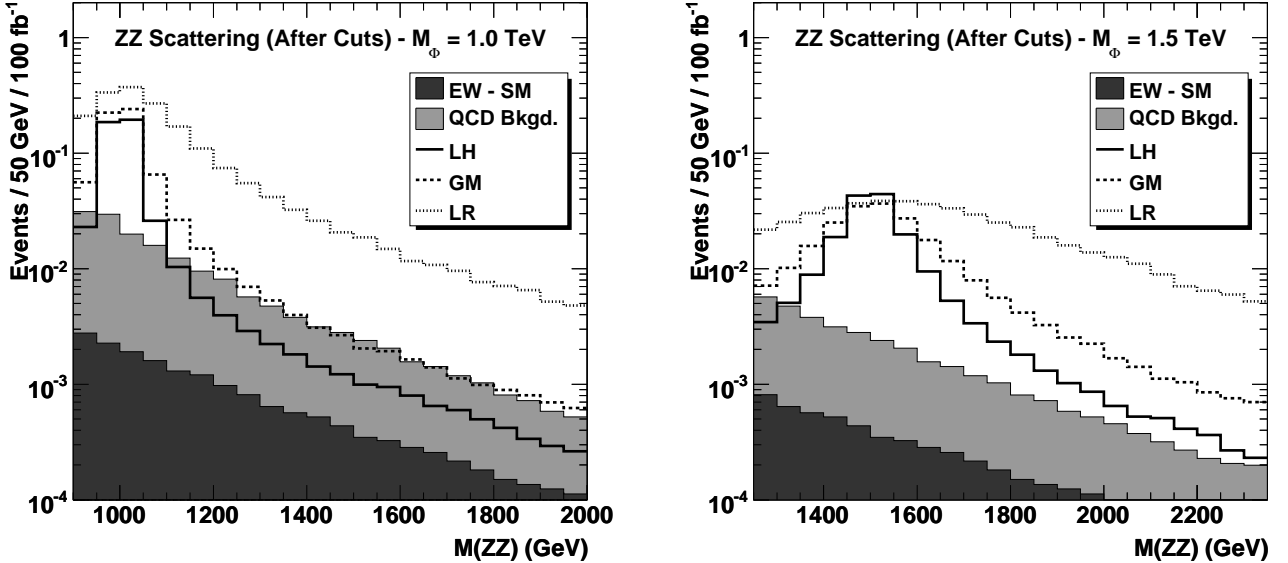


FIG. 6: The invariant mass distributions for ZZ scattering in the Littlest Higgs (LH), Georgi-Machacek (GM) and Left-Right Symmetric (LR) models, along with the backgrounds, after imposing the cuts of Table II. Higgs triplet masses of $M_\Phi = 1.0$ and 1.5 TeV were used, along with a triplet vev of $v' = 39$ GeV, assuming an integrated luminosity of $\mathcal{L} = 100 \text{ fb}^{-1}$. Note that the backgrounds are stacked, whereas the signal lines are not.

TABLE III: The partial widths of the Higgs triplet bosons for the models studied in this paper. The widths are in GeV.

Decay	Littlest Higgs		Georgi-Machacek		Left-Right Symmetric	
	$M_\Phi = 1.0$ TeV	$M_\Phi = 1.5$ TeV	$M_\Phi = 1.0$ TeV	$M_\Phi = 1.5$ TeV	$M_\Phi = 1.0$ TeV	$M_\Phi = 1.5$ TeV
	(GeV)	(GeV)	(GeV)	(GeV)	(GeV)	(GeV)
$\Gamma(\Phi^{\pm\pm} \rightarrow W^\pm W^\pm)$	64	220	64	220	64	220
$\Gamma(\Phi^\pm \rightarrow W^\pm Z)$	32	110	63	220	32	110
$\Gamma(\Phi^\pm \rightarrow W^\pm h)$	42	150	-	-	-	-
$\Gamma(\Phi^0 \rightarrow W^+ W^-)$	-	-	21	73	64	220
$\Gamma(\Phi^0 \rightarrow ZZ)$	31	110	42	150	126	440

between the EW-SM cross section and the EW-LH, EW-GM, and EW-LR cross sections respectively, as defined by Equation 18.

The observability of a Higgs triplet signal in a VV channel is determined by the relative size of the signal to background, and by the assumed integrated luminosity. So, for example, in the Littlest Higgs model with $M_\Phi = 1.0$ TeV and $v' = 39$ GeV, the cross section after cuts in the $W^\pm W^\pm$ channel is 0.244 fb, compared to the cross section of the combined backgrounds of 0.0798 fb. Assuming 100 fb^{-1} , this would result in roughly a 9σ effect. One could invert this and ask what luminosity would be required to produce a 5σ discovery (i.e. $S/\sqrt{B} \geq 5$). For this example, the luminosity required would be 34 fb^{-1} , resulting in ~ 8 signal events. It may be possible to further optimize our cuts in order to enhance the event rate at the expense of lowering the signal to background ratio. In any case, there is a trade-off and this would also depend on detector details that are beyond the scope of this paper. To ensure that a substantial number of signal events are observed, we impose a second criteria that there must be at least 10 signal events, resulting in a required integrated luminosity of 41 fb^{-1} . Following this procedure, in Table V we give the integrated luminosities required to produce a 5σ signal with at least 10 signal events for the various models for triplet masses of 1.0 and 1.5 TeV.

The early years of LHC running are expected to produce $\sim 10 \text{ fb}^{-1}/\text{year}$. It is therefore unlikely that a heavy Higgs triplet would be observed at the LHC in this period of time. Once design luminosity is achieved, it is expected that $\sim 100 \text{ fb}^{-1}$ will be produced per year. In this case it should be possible to observe a doubly-charged Higgs triplet in any of these models with the assumed parameter values. In the $W^\pm Z$ channel, it seems that only the charged scalar in the Georgi-Machacek model could be observed. The $W^+ W^-$ channel is the least promising for observing a Higgs triplet due to the large QCD and t -quark backgrounds in this channel.

The values in Tables IV and V were obtained assuming a triplet vev of $v' = 39$ GeV, which is the upper bound in the Georgi-Machacek model. However, in the Littlest Higgs model this parameter is constrained to $v' \lesssim 4$ GeV, while in the Left-Right Symmetric model the constraint

is $v' \lesssim 2$ GeV. The Higgs triplet production cross section is proportional to v'^2 , so, with these upper limits, the cross sections would be reduced by a factor of roughly 10^{-2} and 2×10^{-3} for the Littlest Higgs and Left-Right Symmetric models respectively. With the resulting cross section values, it is clear that to observe any of the TeV-scale Higgs triplet bosons of the Littlest Higgs or Left-Right Symmetric models at the LHC using leptonic final states would require several ab^{-1} of integrated luminosity and would await the SLHC. However, as is usual in model building, it is possible that the existing constraints could be evaded, making these processes more useful than we pessimistically conclude.

VI. SUMMARY

In this paper, we presented the results of a study of Higgs triplet production via vector boson scattering at the LHC. The production cross sections are highly sensitive to the triplet vacuum expectation value (v') which is already tightly constrained by precision electroweak data. Of the three models considered, the Georgi-Machacek model can have the largest cross sections due to the weakest constraint on v' . The $W^\pm W^\pm$ channel is the most promising discovery channel due to its distinctive final state. However, it is still possible to observe a signal for the $W^\pm Z$ channel for certain regions of parameter space. The observation of this channel is a smoking gun for a Higgs triplet, as this process does not occur in Two Higgs Doublet Models. Discovery of the neutral Higgs triplet state is least promising due to the large QCD and t -quark backgrounds in the $W^+ W^-$ channel and the small signal cross section in the $ZZ \rightarrow l^+ l^- l^+ l^-$ channel. The $ZZ \rightarrow l^+ l^- \nu \bar{\nu}$ channel might slightly improve the Φ^0 discovery potential, but we have not included this in our analysis and leave this for a future study. High luminosity is required for some of the channels and models, which will require the SLHC.

One of the goals of this work was to determine whether scalar triplet production via vector boson scattering at the LHC could be used to distinguish between models with Higgs triplet bosons. Our conclusions are qualified. The current constraints on the triplet vev in the Littlest

TABLE IV: LHC cross sections (in fb) for vector boson scattering using the cuts listed in Table II. The cross sections are shown for the three models we are considering, using a triplet vev of $v' = 39$ GeV and Higgs triplet masses of $M_\Phi = 1.0$ TeV (left-hand columns) and $M_\Phi = 1.5$ TeV (right-hand columns). The cross section values obtained using MadGraph are accurate to $\sim 1\%$.

Process	$M_\Phi = 1.0$ TeV			$M_\Phi = 1.5$ TeV		
	Leptonic Cuts	+ Jet Tag	+ Jet Veto	Leptonic Cuts	+ Jet Tag	+ Jet Veto
$W^\pm W^\pm$						
EW - LH	9.39×10^{-1}	3.03×10^{-1}	2.55×10^{-1}	2.92×10^{-1}	1.05×10^{-1}	8.85×10^{-2}
EW - GM	9.41×10^{-1}	3.06×10^{-1}	2.56×10^{-1}	2.88×10^{-1}	1.03×10^{-1}	8.75×10^{-2}
EW - LR	9.36×10^{-1}	3.04×10^{-1}	2.56×10^{-1}	2.91×10^{-1}	1.04×10^{-1}	8.87×10^{-2}
EW - SM	2.01×10^{-1}	1.57×10^{-2}	1.06×10^{-2}	6.48×10^{-2}	4.91×10^{-3}	3.42×10^{-3}
QCD Bkgd.	1.16×10^{-1}	7.90×10^{-4}	4.22×10^{-4}	4.51×10^{-2}	2.47×10^{-4}	1.67×10^{-4}
t -quark Bkgd.	4.42×10^{-1}	8.15×10^{-4}	5.52×10^{-4}	1.29×10^{-1}	1.38×10^{-4}	7.33×10^{-5}
$W^\pm Z$ Bkgd.	5.75	8.58×10^{-2}	6.82×10^{-2}	1.45	1.91×10^{-2}	1.67×10^{-2}
Total Bkgd.	6.51	1.03×10^{-1}	7.98×10^{-2}	1.69	2.44×10^{-2}	2.04×10^{-2}
Signal - LH	7.38×10^{-1}	2.87×10^{-1}	2.44×10^{-1}	2.27×10^{-1}	1.00×10^{-1}	8.51×10^{-2}
Signal - GM	7.40×10^{-1}	2.90×10^{-1}	2.45×10^{-1}	2.23×10^{-1}	0.98×10^{-1}	8.41×10^{-2}
Signal - LR	7.35×10^{-1}	2.88×10^{-1}	2.45×10^{-1}	2.26×10^{-1}	0.99×10^{-1}	8.53×10^{-2}
$W^\pm Z$						
EW - LH	9.50×10^{-2}	1.95×10^{-2}	1.56×10^{-2}	3.12×10^{-2}	6.84×10^{-3}	5.48×10^{-3}
EW - GM	2.44×10^{-1}	7.46×10^{-2}	6.15×10^{-2}	7.86×10^{-2}	2.66×10^{-2}	2.22×10^{-2}
EW - LR	1.51×10^{-1}	4.01×10^{-2}	3.28×10^{-2}	5.13×10^{-2}	1.51×10^{-2}	1.25×10^{-2}
EW - SM	5.47×10^{-2}	4.47×10^{-3}	3.03×10^{-3}	1.87×10^{-2}	1.60×10^{-3}	1.06×10^{-3}
QCD Bkgd.	1.60	1.96×10^{-2}	1.72×10^{-2}	3.34×10^{-1}	2.60×10^{-3}	2.25×10^{-3}
t -quark Bkgd.	2.54×10^{-1}	1.02×10^{-3}	7.30×10^{-4}	5.62×10^{-2}	1.07×10^{-4}	8.93×10^{-5}
Total Bkgd.	1.91	2.51×10^{-2}	2.10×10^{-2}	4.09×10^{-1}	4.31×10^{-3}	3.40×10^{-3}
Signal - LH	4.03×10^{-2}	1.50×10^{-2}	1.26×10^{-2}	1.25×10^{-2}	5.24×10^{-3}	4.42×10^{-3}
Signal - GM	1.89×10^{-1}	7.01×10^{-2}	5.85×10^{-2}	5.99×10^{-2}	2.50×10^{-2}	2.11×10^{-2}
Signal - LR	0.96×10^{-1}	3.56×10^{-2}	2.98×10^{-2}	3.26×10^{-2}	1.35×10^{-2}	1.14×10^{-2}
$W^+ W^-$						
EW - LH	-	-	-	-	-	-
EW - GM	1.62×10^{-1}	2.08×10^{-2}	9.91×10^{-3}	7.28×10^{-2}	9.20×10^{-3}	4.35×10^{-3}
EW - LR	2.35×10^{-1}	4.63×10^{-2}	2.28×10^{-2}	9.70×10^{-2}	1.84×10^{-2}	9.23×10^{-3}
EW - SM	1.32×10^{-1}	1.07×10^{-2}	4.75×10^{-3}	5.98×10^{-2}	4.32×10^{-3}	1.79×10^{-3}
QCD Bkgd.	4.72	1.61×10^{-2}	4.29×10^{-3}	9.18×10^{-1}	3.13×10^{-3}	8.34×10^{-4}
t -quark Bkgd.	5.70×10^1	5.16×10^{-2}	1.48×10^{-2}	1.28×10^1	1.18×10^{-2}	3.99×10^{-3}
Total Bkgd.	6.18×10^1	7.84×10^{-2}	2.38×10^{-2}	1.38×10^1	1.92×10^{-2}	6.61×10^{-3}
Signal - LH	-	-	-	-	-	-
Signal - GM	0.30×10^{-1}	1.01×10^{-2}	5.16×10^{-3}	1.30×10^{-2}	4.88×10^{-3}	2.56×10^{-3}
Signal - LR	1.03×10^{-1}	3.56×10^{-2}	1.80×10^{-2}	3.72×10^{-2}	1.41×10^{-2}	7.44×10^{-3}
ZZ						
EW - LH	1.59×10^{-2}	4.67×10^{-3}	-	5.58×10^{-3}	1.78×10^{-3}	-
EW - GM	2.12×10^{-2}	6.77×10^{-3}	-	7.01×10^{-3}	2.38×10^{-3}	-
EW - LR	5.28×10^{-2}	1.86×10^{-2}	-	1.51×10^{-2}	5.87×10^{-3}	-
EW - SM	3.20×10^{-3}	1.83×10^{-4}	-	1.30×10^{-3}	4.80×10^{-5}	-
QCD Bkgd.	8.00×10^{-2}	1.50×10^{-3}	-	1.67×10^{-2}	3.49×10^{-4}	-
Total Bkgd.	8.32×10^{-2}	1.68×10^{-3}	-	1.80×10^{-2}	3.97×10^{-4}	-
Signal - LH	1.27×10^{-2}	4.49×10^{-3}	-	4.28×10^{-3}	1.73×10^{-3}	-
Signal - GM	1.80×10^{-2}	6.59×10^{-3}	-	5.71×10^{-3}	2.33×10^{-3}	-
Signal - LR	4.96×10^{-2}	1.84×10^{-2}	-	1.38×10^{-2}	5.82×10^{-3}	-

TABLE V: The integrated luminosity (in fb^{-1}) required for a statistical significance of $S/\sqrt{B} \geq 5$ and at least 10 signal events, after the cuts of Table II have been imposed. These results were obtained for a triplet vev of $v' = 39$ GeV, using the cross section values listed in Table IV.

Channel	Littlest Higgs		Georgi-Machacek		Left-Right Symmetric	
	$M_\Phi = 1.0$ TeV (fb^{-1})	$M_\Phi = 1.5$ TeV (fb^{-1})	$M_\Phi = 1.0$ TeV (fb^{-1})	$M_\Phi = 1.5$ TeV (fb^{-1})	$M_\Phi = 1.0$ TeV (fb^{-1})	$M_\Phi = 1.5$ TeV (fb^{-1})
$W^\pm W^\pm$	41	118	41	119	41	117
$W^\pm Z$	3300	4350	171	474	591	877
$W^+ W^-$	-	-	22300	25200	1840	2980
ZZ	2230	5780	1520	4290	543	1720

Higgs and Left-Right Symmetric models result in production cross sections that would require significant luminosity to be able to distinguish triplet scalars from Standard Model backgrounds, higher than the expected LHC luminosities. In these scenarios, these measurements could at best constrain the allowed parameter space. However, if the $W^\pm W^\pm$ and $W^\pm Z$ signals are observed, it would be possible to distinguish the three models we studied by computing the ratio of the rates in those two channels. In doing so, the dependence on the triplet vev cancels out, and this ratio would be sensitive to the details each model.

We focused our work on the fully leptonic final states, which are easiest to distinguish from Standard Model backgrounds. The “silver-plated” semileptonic decay modes have significantly higher branching ratios and could potentially improve the statistics; the branching ratios are $\mathcal{B}(W^\pm W^\pm \rightarrow l^\pm \nu l^\pm \nu) \sim 5\%$ versus $\mathcal{B}(W^\pm W^\pm \rightarrow l^\pm \nu q \bar{q}) \sim 29\%$, $\mathcal{B}(W^\pm Z \rightarrow l^\pm \nu l^\pm l^-) \sim$

1.5% versus $\mathcal{B}(W^\pm Z \rightarrow l^\pm \nu q \bar{q} + q \bar{q} l^\pm l^-) \sim 20\%$, and $\mathcal{B}(ZZ \rightarrow l^+ l^- l^+ l^-) \sim 0.44\%$ versus $\mathcal{B}(ZZ \rightarrow l^+ l^- q \bar{q}) \sim 9\%$. However, much depends on the efficiency in reconstructing W and Z bosons in their hadronic modes. In addition, the kinematic cuts would need to be modified to take into account the hadronic final states. We leave this exercise for a future study.

Acknowledgments

The authors gratefully acknowledge P. Kalyniak for her suggestion that led to this work and H. Logan for her numerous comments and suggestions that greatly improved this paper. We also thank H. Hou, D. Morrissey, and J. Reuter for helpful discussions and communications. This research was supported in part by the Natural Sciences and Engineering Research Council of Canada.

-
- [1] D. E. Morrissey, T. Plehn and T. M. P. Tait, arXiv:0912.3259 [hep-ph].
 - [2] E. Accomando *et al.*, arXiv:hep-ph/0608079.
 - [3] P. Nath *et al.*, arXiv:1001.2693 [hep-ph].
 - [4] N. Arkani-Hamed, A. G. Cohen, E. Katz and A. E. Nelson, JHEP **0207**, 034 (2002) [arXiv:hep-ph/0206021].
 - [5] G. Burdman, M. Perelstein and A. Pierce, Phys. Rev. Lett. **90**, 241802 (2003) [Erratum-ibid. **92**, 049903 (2004)] [arXiv:hep-ph/0212228].
 - [6] T. Han, H. E. Logan, B. McElrath and L. T. Wang, Phys. Rev. D **67**, 095004 (2003) [arXiv:hep-ph/0301040].
 - [7] T. Han, H. E. Logan and L. T. Wang, JHEP **0601**, 099 (2006) [arXiv:hep-ph/0506313].
 - [8] M. Perelstein, Prog. Part. Nucl. Phys. **58**, 247 (2007) [arXiv:hep-ph/0512128].
 - [9] G. Azuelos *et al.*, Eur. Phys. J. C **39S2**, 13 (2005) [arXiv:hep-ph/0402037].
 - [10] J. Hubisz and P. Meade, Phys. Rev. D **71**, 035016 (2005) [arXiv:hep-ph/0411264].
 - [11] E. Asakawa, S. Kanemura and J. Kanzaki, Phys. Rev. D **75**, 075022 (2007) [arXiv:hep-ph/0612271].
 - [12] H. Georgi and M. Machacek, Nucl. Phys. B **262**, 463 (1985)
 - [13] R. N. Mohapatra and J. C. Pati, Phys. Rev. D **11**, 566 (1975)
 - [14] G. Senjanovic and R. N. Mohapatra, Phys. Rev. D **12**, 1502 (1975).
 - [15] P. H. Frampton, Phys. Rev. Lett. **69**, 2889 (1992).
 - [16] F. Pisano and V. Pleitez, Phys. Rev. D **46**, 410 (1992) [arXiv:hep-ph/9206242].
 - [17] J. E. Cieza Montalvo, N. V. Cortez, J. Sa Borges and M. D. Tonasse, Nucl. Phys. B **756**, 1 (2006) [Erratum-ibid. B **796**, 422 (2008)] [arXiv:hep-ph/0606243].
 - [18] C. Csaki, C. Grojean, H. Murayama, L. Pilo and J. Terning, Phys. Rev. D **69**, 055006 (2004) [arXiv:hep-ph/0305237].
 - [19] C. Csaki, C. Grojean, L. Pilo and J. Terning, Phys. Rev. Lett. **92**, 101802 (2004) [arXiv:hep-ph/0308038].
 - [20] A. S. Belyaev, R. Sekhar Chivukula, N. D. Christensen, H. J. He, M. Kurachi, E. H. Simmons and M. Tanabashi, arXiv:0907.2662 [hep-ph].
 - [21] H. J. He *et al.*, Phys. Rev. D **78**, 031701 (2008) [arXiv:0708.2588 [hep-ph]].
 - [22] A. Alves, O. J. P. Eboli, D. Goncalves, M. C. Gonzalez-

- Garcia and J. K. Mizukoshi, arXiv:0907.2915 [hep-ph].
- [23] A. Birkedal, K. Matchev and M. Perelstein, Phys. Rev. Lett. **94**, 191803 (2005) [arXiv:hep-ph/0412278].
 - [24] K. Cheung, C. W. Chiang and T. C. Yuan, Phys. Rev. D **78**, 051701 (2008) [arXiv:0803.2661 [hep-ph]].
 - [25] I. Dorsner and I. Mocioiu, Nucl. Phys. B **796**, 123 (2008) [arXiv:0708.3332 [hep-ph]].
 - [26] T. Han, H. E. Logan, B. Mukhopadhyaya and R. Srikanth, Phys. Rev. D **72**, 053007 (2005) [arXiv:hep-ph/0505260].
 - [27] J. F. Gunion, R. Vega and J. Wudka, Phys. Rev. D **42**, 1673 (1990).
 - [28] K. Huitu, J. Maalampi, A. Pietila and M. Raidal, Nucl. Phys. B **487**, 27 (1997) [arXiv:hep-ph/9606311].
 - [29] J. F. Gunion, J. Grifols, A. Mendez, B. Kayser and F. I. Olness, Phys. Rev. D **40**, 1546 (1989).
 - [30] G. Azuelos, K. Benslama and J. Ferland, J. Phys. G **32**, 73 (2006) [arXiv:hep-ph/0503096].
 - [31] V. D. Barger, K. m. Cheung, T. Han and R. J. N. Phillips, Phys. Rev. D **42**, 3052 (1990).
 - [32] J. Bagger *et al.*, Phys. Rev. D **49**, 1246 (1994) [arXiv:hep-ph/9306256].
 - [33] J. Bagger *et al.*, Phys. Rev. D **52**, 3878 (1995) [arXiv:hep-ph/9504426].
 - [34] W. B. Kilgore, *In the Proceedings of 1996 DPF / DPB Summer Study on New Directions for High-Energy Physics (Snowmass 96), Snowmass, Colorado, 25 Jun - 12 Jul 1996, pp STC132* [arXiv:hep-ph/9610375].
 - [35] M. Schmaltz and D. Tucker-Smith, Ann. Rev. Nucl. Part. Sci. **55**, 229 (2005) [arXiv:hep-ph/0502182].
 - [36] N. Arkani-Hamed, A. G. Cohen and H. Georgi, Phys. Lett. B **513**, 232 (2001) [arXiv:hep-ph/0105239].
 - [37] M. Perelstein, Prog. Part. Nucl. Phys **58**, 247 (2007) [arXiv:hep-ph/0512128v1].
 - [38] M.-C. Chen and S. Dawson, Phys. Rev. D **70**, 015003 (2004) [arXiv:hep-ph/0311032v3].
 - [39] H. Haber and H. Logan, Phys. Rev. D **62**, 015011 (2000).
 - [40] N. G. Deshpande, J. F. Gunion, B. Kayser and F. I. Olness, Phys. Rev. D **44**, 837 (1991).
 - [41] C. Amsler *et al.* [Particle Data Group], Phys. Lett. B **667**, 1 (2008).
 - [42] J. Alwall *et al.*, JHEP **0709**, 028 (2007) [arXiv:0706.2334 [hep-ph]].
 - [43] S. Dawson, Nucl. Phys. B **249**, 42 (1985).
 - [44] J. Cornwall, D. Levin and G. Tiktopoulos, Phys. Rev. D **10**, 1145 (1974).
 - [45] K. Moats, M.Sc. thesis Carleton University (2007).
 - [46] T. Han, D. Krohn, L. T. Wang and W. Zhu, JHEP **1003**, 082 (2010) [arXiv:0911.3656 [hep-ph]].
 - [47] V. D. Barger, A. D. Martin and R. J. N. Phillips, Phys. Lett. B **125**, 339 (1983).
 - [48] V. D. Barger, T. Han and J. Ohnemus, Phys. Rev. D **37**, 1174 (1988).
 - [49] J. Pumplin *et al.*, JHEP **0207**, 012 (2002).
 - [50] P. Meade and M. Reece, arXiv:hep-ph/0703031.